*metals*

MDPI

*Article*

# Fabrication, Experimental Investigation and Prediction of Wear Behavior of Open-Cell AlSi10Mg-SiC Composite Materials

**Mihail Kolev *, Ludmil Drenchev and Veselin Petkov**

Institute of Metal Science, Equipment and Technologies with Center for Hydro- and Aerodynamics "Acad. A. Balevski", Bulgarian Academy of Sciences, 1574 Sofia, Bulgaria; ljudmil.d@ims.bas.bg (L.D.)
* Correspondence: mihail1kolev@gmail.com

**Abstract:** This research investigates the tribological behavior of advanced open-cell porous AlSi10Mg-SiC composites fabricated using the novel replication method of NaCl space holders. These composite materials have potential applications in lightweight and high-strength structures that require high resistance to friction and wear. The composites were tested using a pin-on-disk method under dry sliding-friction conditions at ambient temperature, with a sliding velocity of 1.0 $m \cdot s^{-1}$ and an applied load of 50 N. The resulting wear parameters, including the coefficient of friction (COF) and mass wear, provided quantitative measures of the tribological behavior. Microstructural observations of the worn composite surfaces were carried out using scanning-electron microscopy (SEM) to study the wear mechanisms, and an elemental analysis was performed using X-ray energy-dispersive spectroscopy (EDS) to examine the elemental composition. The results showed that the AlSi10Mg-SiC composites had lower mass wear and COF than the open-cell porous AlSi10Mg material under the same experimental conditions. Three different machine learning (ML) models were employed to predict the COF of the composites, and their performances were evaluated using the R2, MSE, RMSE, and MAE metrics on the validation and test sets.

**Keywords:** AlSi10Mg-SiC; aluminum-metal-matrix composites; wear behavior; mass wear; coefficient of friction; machine-learning models



**Citation:** Kolev, M.; Drenchev, L.; Petkov, V. Fabrication, Experimental Investigation and Prediction of Wear Behavior of Open-Cell AlSi10Mg-SiC Composite Materials. *Metals* **2023**, *13*, 814. https://doi.org/10.3390/met13040814

Academic Editor: Slobodan Mitrovic

Received: 29 March 2023
Revised: 9 April 2023
Accepted: 18 April 2023
Published: 21 April 2023



## 1. Introduction

Due to their distinctive characteristics and versatile applications across different domains, composite materials have attracted considerable interest and attention. In this regard, researchers have explored different methods with which to fabricate advanced composite materials with enhanced properties. One of these methods is the replication of NaCl space holders, which allows precise control over the porosity and morphology of the resulting composite material [1–3].

Researchers have conducted extensive studies on open-cell aluminum-metal-matrix composites (AMMCs) due to their remarkable properties, which have found widespread applications in various functional and structural engineering applications. For instance, AMMCs that are reinforced with graphite are used to develop wear-resistant and lightweight cylinder liners for internal combustion engines [4]. Furthermore, AMMCs that are reinforced with SiC are employed in the manufacturing of energy-saving brake rotors used in automobiles due to their high thermal conductivity and wear resistance [5].

The replication method is one of the most commonly employed processes for producing AMMCs due to its simplicity in the experimental part and the high level of control it offers over the size, form, and pore distribution of the final porous AMMC structure (AMMC skeleton) [6]. This method involves the fabrication of a preform, which may be composed of various space holders, such as carbamide [7], NaCl [8–13], magnesium [14], Acrowax [15], ammonium bicarbonate [16], saccharose [17], and potassium carbonate [18]. Among these space holders, NaCl is one of the most prominent; it has been extensively studied and used in the fabrication of porous metal structures.

Various types of reinforcing phase (RP) are incorporated to enhance the hardness and wear resistance of the softer matrix in AMMCs. Ceramic materials, such as silicon carbide (SiC) [19–22], alumina ($Al_2O_3$) [19,23–25], boron carbide ($B_4C$) [26], titanium carbide (TiC) [27,28], and graphite (Gr) [29,30] are some of the most commonly used RP materials due to their excellent tribological behavior. In particular, SiC is an appropriate option for reinforcing AMMCs due to its high tensile and compressive strength, hardness, stiffness, and thermal stability, as well as its excellent wear resistance.

Liquid-state processing is a widely used method for the production of AMMCs due to its cost-effectiveness and the ability it offers to distribute reinforcement effectively. This method involves mixing the metal matrix and reinforcement material in a liquid state, which allows the uniform distribution of the reinforcement material throughout the matrix. Additionally, this process enables the use of a wide range of reinforcement materials with varying properties, shapes, and sizes, which provides flexibility in the design of composites. By using the liquid-state-processing technique, it is possible to manufacture intricate geometries and near-net-shaped components, resulting in decreased material wastage and machining expenses. These advantages make liquid-state processing a popular and efficient method for the fabrication of AMMCs [31–33].

The authors of [34] investigated the effect of combined squeeze-casting and stir-casting processes on the microstructural, mechanical, and wear properties of Al5083 reinforced with 20–30 wt. % $SiC_p$. The experimental findings indicated that the combination of casting techniques enhanced the dispersion of the $SiC_p$, minimized the porosity, and improved the mechanical and wear properties in comparison to using only the stir-casting method. The primary wear mechanism observed in all the composites was the delamination of the friction layer. Khadijeh M. et al. [35] were successful in synthesizing AMMCs using a process that involved the pressure-assisted melt infiltration of Al into SiC preforms. The addition of water to the process led to improved wetting and bonding between the metal and preform, resulting in AMMCs with higher compressive-strength values compared to other materials. The composites demonstrated elevated levels of hardness, with the Al-SiC (75 wt. %) composite displaying the greatest compressive strength. This strength was attributed to the Orowan strengthening mechanism. Furthermore, the development of a tribological layer on the surfaces of the Al-SiC (67 wt. %) and the Al-SiC (75 wt. %) resulted in improved wear resistance in comparison to the Al alloy. According to Jiang W et al. [36] the addition of 2 wt. % of SiC particles as reinforcements combined with the use of squeeze casting is an effective way to improve the tensile and yield strength, as well as the hardness, of 6082 aluminum alloys due to the more uniform distribution of the reinforcement. Du Yuan and Xiong Yang [37] reported the development of high-strength and high-toughness nano-SiCp/A356 composites using ultrasonic vibration and squeeze-casting techniques, demonstrating that the addition of 2 wt. % nano-sized SiC particles significantly improves the mechanical properties of composite materials. The study by V. Chakkravarthy et al. [38] revealed that the addition of TiN, SiC, and Nb particles improves the microhardness and wear resistance of composite materials. Their study concludes that the microstructural changes induced by the addition of these particles are responsible for improvements in the mechanical properties and wear resistance of composite materials. The authors Navya Kota et al. [39] reviewed the current status and applications of interpenetrating phase composites (IPCs), discussed various processing routes for fabricating open porous ceramic preforms, and evaluated different melt-infiltration techniques based on the results presented by other authors. They summarized that Al-Si/SiC IPCs can be fabricated by infiltrating SiC foams obtained via the replication method using Al-Si alloys through the squeeze-casting method. The composites showed significant improvements in hardness compared to the unreinforced Al-Si alloy, with the finer-pore-size foam composite demonstrating the greatest hardness. The SEM analysis confirmed a well-bonded interface with no intermediate reaction products.

Machine learning (ML) is an area of artificial intelligence that helps computer systems to enhance their performances through experience and without the requirement of explicit

programming. It involves the development of algorithms and statistical models that can analyze and draw insights from data to make predictions or decisions. Machine learning has been widely applied in different fields for over two decades, and these applications have expanded beyond computer science. In particular, the integration of ML and material science has enabled the prediction of output measurements, such as hardness [40], tensile strength [41], the volume loss of AA7075-$Al_2O_3$ composites [23], and the additive manufacturing of AlSi10Mg-TiCN composites with tailorable mechanical behavior [42]. By utilizing machine-learning techniques, scientists and engineers can analyze complex data sets to make predictions about the behavior of materials, improving the efficiency and effectiveness of materials research. Furthermore, ML methods can produce encouraging outcomes with relatively small datasets, even though they necessitate substantial amounts of data. However, further elaborations on the specific applications and benefits of machine learning in various fields could help to provide a more comprehensive understanding of its utility.

The aim of this study was to investigate the tribological behavior of open-cell AlSi10Mg-SiC composites that were produced using a novel fabrication technique. The pin-on-disk method was employed to evaluate the wear parameters, including the mass wear and coefficient of friction (COF), under dry sliding-friction conditions at ambient temperature. Scanning-electron microscopy (SEM) was also conducted to investigate the wear mechanisms, while the elemental composition of the composites was examined using X-ray energy-dispersive spectroscopy (EDS). The results of this study provide valuable insights into the potential applications of AlSi10Mg-SiC composites and their tribological behavior under specific working conditions.

In addition, machine-learning algorithms were utilized to predict the COF of the AlSi10Mg-SiC composites under dry sliding conditions. Three different ML models, namely Random Forest, Decision Tree, and Extreme Gradient Boosting, were implemented to predict the wear behavior of the composites. The performances of these models were evaluated on the validation and test sets using various metrics, such as the coefficient of determination (R2), mean squared error (MSE), root mean squared Error (RMSE), and mean absolute error (MAE).

The AlSi10Mg alloy has good castability, high strength, and excellent corrosion resistance. On the other hand, SiC is recognized for its exceptional strength, hardness, and stiffness. The combination of the squeeze-casting process and the incorporation of SiC particles into the AlSi10Mg matrix produced a porous open-cell-composite test specimen with enhanced tribological and mechanical properties, making it suitable for a range of applications, such as the production of slide-contact bearings. This research builds upon previous studies in which open-cell AMMCs were produced employing the replication method [43], and their skeletons were infiltrated with tin-based babbitt [12,13,44,45].

## 2. Materials and Methods

### *2.1. Production Method and Materials*

The production process of open-cell AlSi10Mg-SiC composite (composite skeleton) is illustrated in Figure 1. The fabrication process involved the replication method for the preparation of the preliminary preform and squeeze casting for the infiltration of the obtained preliminary preform with AlSi10Mg alloy. The process of fabricating the composite skeleton started with the preparation of the preliminary preform with the desired porosity, via the replication method.

To obtain the preliminary preform, a mixture of 5 wt. % SiC particles, 6 wt. % water, and NaCl particles used as soluble space holder was homogenized in a 3D powder blender. The homogenized mixture was then compressed with a pressure of 1.5 MPa into a steel cylinder. The "green" compacts were first dried in a furnace at 200 °C for 2 h to remove moisture. Subsequently, the green dried compacts were sintered in a furnace at 800 °C ± 1 °C for 1 h, followed by cooling at room temperature to obtain the salt leachable preform.

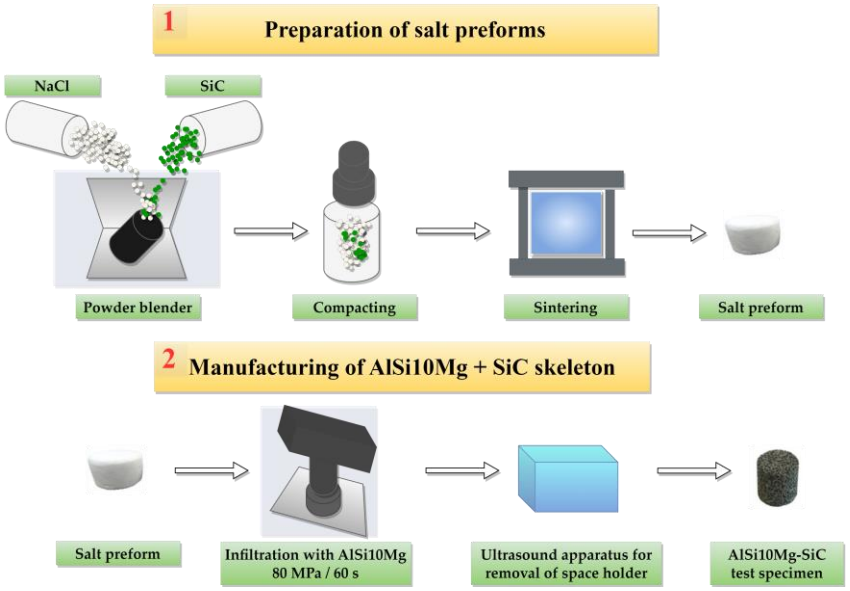


**Figure 1.** Production process of open-cell AlSi10Mg-SiC composite.

The process continued with the infiltration of the NaCl preforms with the Al-based alloy. The salt preforms were preheated and positioned in a die at a temperature of 680 °C ± 2 °C, following which they were subjected to infiltration by molten AlSi10Mg alloy using the squeeze-casting method. An applied pressure of 80 MPa for 60 s was used during the process. The molten alloy filled the voids in the salt preform, resulting in the formation of the AlSi10Mg-SiC skeleton.

After cooling down to room temperature, the obtained composite material was subjected to removal of the space holder via dissolution in hot distilled water at a temperature of 70 °C using an ultrasonic apparatus. The resulting open-cell AlSi10Mg-SiC composite exhibited a high strength-to-weight ratio, excellent corrosion and wear resistance, and good thermal and electrical conductivity. This composite has diverse applications across multiple industries, including aerospace, automotive, and biomedical, due to its unique combination of properties.

The AlSi10Mg alloy (refer to Table 1) was chosen based on its desirable characteristics, including its light weight, flexibility during post-processing, and excellent thermal and mechanical properties. The reinforcement of the material was achieved by incorporating SiC particles that ranged in size from 300 to 400 μm. To control the sizes of the pores, NaCl particles with a size range of 800 to 1000 μm were employed.

**Table 1.** AlSi10Mg-alloy composition.

| Element | Si | Fe | Cu | Mn | Mg | Ni | Zn | Pb | Sn | Ti | Al |
|---|---|---|---|---|---|---|---|---|---|---|---|
| Concentration, wt. % | 9.0–11.0 | 0.55 | 0.05 | 0.45 | 0.2–0.45 | 0.05 | 0.10 | 0.05 | 0.05 | 0.15 | rest |

### *2.2. Characterization Methods*

Ducom Rotary (Pin/Ball-on-Disk) tribometer, TR-20 Ducom model (Ducom Instruments Pvt. Ltd. Ducom, Bangalore, India), was utilized to determine the wear properties of all test specimens. A pin-on-disk system was employed to carry out dry-wear tests on test specimens. The specimens were machined by lathe to achieve the desired height and diameter dimensions for the wear test. The test specimens were prepared with a spherical tip and machined to the desired dimensions of 20 mm in height and 10 mm in diameter. The wear-test parameters included a linear velocity of 1.0 $m \cdot s^{-1}$, a load of 50 N, and sliding distance of 420 m. The data-acquisition system of the tribological equipment was used to calculate the coefficient of friction (COF). The wear experiments were conducted using a

counter disk of EN-31 steel hardened to 62 HRC and with a diameter of 140 mm (surface roughness: 1.6 Ra) (refer to Table 2).

**Table 2.** EN-31-steel composition.

| Element | C | Si | Mn | Cr | Si | Fe |
|---|---|---|---|---|---|---|
| Concentration, wt. % | 0.90–1.20 | 0.10–0.35 | 0.30–0.75 | 1.00–1.60 | 0.20 | rest |

The worn surfaces of the AlSi10Mg-SiC composites after the wear tests were examined using scanning-electron microscopy (SEM), SH-5500P model (Hirox Japan Co. Ltd. Hirox, Tokyo, Japan). The SEM images provided valuable insights into the types of wear that occurred, such as adhesive wear and abrasive wear. These wear mechanisms complemented the wear-parameter measurements, such as coefficient of friction and mass wear, and helped to provide a more comprehensive understanding of the tribological behavior of the composites. For chemical micro-analysis, an X-ray energy-dispersive spectroscopy (EDS) system, QUANTAX 100 Advanced model (BRUKER, Kontich, Belgium Bruker), was used. For the homogenization of the space-holder particles, 3D powder blender—WAB T2F Turbula Heavy-Duty Shaker-Mixer (Willy A. Bachofen AG, Muttenz, Switzerland) was employed.

### *2.3. Approaches for Machine-Learning Models*

Machine-learning models are computational algorithms that learn from data to uncover patterns, insights, and relationships that can be used to make decisions or predictions. In supervised learning, a type of machine learning, these models are trained on labeled data, under conditions in which inputs and the desired outputs are known. One class of supervised-learning algorithm is regression models, which are used to predict continuous numerical values, such as the wear of AMMCs. This study utilizes recent advances in machine learning to predict the coefficient of friction as a function of sliding distance of the AlSi10Mg-SiC skeleton. The approach we take is inspired by the methods outlined in a recent manuscript by Fatih A. et al. [46] on predicting wear. Our objective is to create a ML-based predictive model that can accurately predict the wear behavior of AMMCs with only a limited dataset. As we develop the model, we will continue to expand our dataset and establish correlations between the technological and experimental variables based on the insights we gain from this manuscript, which will be useful for future studies. In this way, we can refine our predictive model and gain a deeper understanding of the relationships between various factors that affect the wear behavior of AMMCs.

This study uses three supervised-machine-learning regression models: Decision Tree (DT) [47], Random Forest (RF) [48], and Extreme Gradient Boosting (XGB) [49]. We compare the results of these models to determine which is the most effective for our purposes. Decision Tree is a non-parametric model that splits data into smaller subgroups based on a set of rules. It works by dividing data into increasingly small subsets based on the input features, until the subsets contain only one class or the prediction of the target variable. The resulting tree can be utilized to make predictions for new data points by following the branches of the tree based on the input feature values. Random Forest is an ensemble model that consists of multiple decision trees. To arrive at a final prediction, the algorithm constructs each decision tree using a subset of the available data and subsequently calculates an average of the predictions made by each tree. This method can help to reduce overfitting and improve the accuracy of predictions. Extreme Gradient Boosting is another ensemble model that consists of multiple weak models, such as Decision Trees, which are trained sequentially. It works by iteratively adding Decision Trees to the model, with each new tree focusing on data points that are not well predicted by the previous trees. The use of this method has the potential to enhance prediction accuracy by reducing the presence of bias and variance in the model. All of these models can be used for prediction of wear of AMMCs, and each has its strengths and weaknesses. The choice of model is based on the distinctive attributes of the data and the desired levels of accuracy and interpretability.

All implementations were coded in the Python programming language. Machine learning involves a set of steps that typically follow a general block diagram (refer to Figure 2). We started by collecting relevant data from the actual pin-on-disk experiments. Once the data were collected, they were preprocessed, which involved cleaning, transforming, and organizing the data before using them for machine learning. The script then trained the model with the best hyperparameters on the training set and evaluated its performance on the validation and test sets using various metrics, such as R2, RMSE, MSE, and MAE. In ML, a model is usually trained on a training set and then evaluated on a separate set of data, which can be either a validation set or a test set. The validation set is used during training to tune hyperparameters and to monitor the performance of the model during the training process. The goal of tuning the hyperparameters is to find the best combination of settings that produces the best performance on the validation set. After the model has been trained and the hyperparameters have been optimized, it is evaluated on a test set to estimate how well it will perform on new, unseen data.

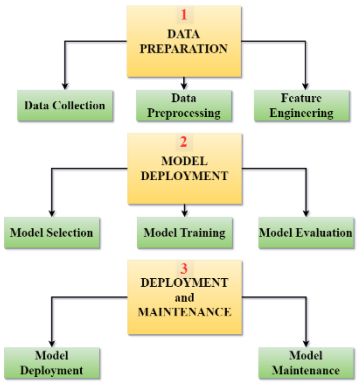


**Figure 2.** Overview of the steps involved in machine learning: a general block diagram.

To ensure consistency and comparability with the findings of Fatih et al. [46], we utilized the hyperparameters they specified for the three machine-learning models described in our study. Specifically, the hyperparameters stated in their manuscript were used to configure the tuning hyperparameters for each model independently, as we intended to identify the optimal configuration for each model.

## 3. Results and Discussion

### *3.1. Microstructure*

The SEM images of the test specimen after the wear tests are presented in Figure 3, with distinct zones indicated by markers, which were taken after conducting tribological experiments with a linear speed of 1.0 m·s$^{-1}$, a load of 50 N, and a sliding distance of 420 m. The analysis results from the EDS can be found in Tables 3 and 4, as well as in Figure 4.

**Table 3.** EDS analysis of the wear surface of AlSi10Mg material in selected zones from Figure 3a, at a load of 50 N and linear speed of 1.0 m·s$^{-1}$, mass norm., %.

| Analysis No. | Al | Fe | Si | Other |
|---|---|---|---|---|
| 1 | 91.28 | 0.68 | 5.53 | rest |
| 2 | 50.03 | 40.94 | 5.12 | rest |

**Table 4.** EDS analysis of the wear surface of AlSi10Mg-SiC skeleton in selected zones from Figure 3b, at a load of 50 N and linear speed of 1.0 m·s$^{-1}$, mass norm., %.

| Analysis No. | Al | Si | Fe | Other |
|---|---|---|---|---|
| 1 | 27.50 | 72.50 | – | – |
| 2 | 54.17 | 7.74 | 37.21 | rest |

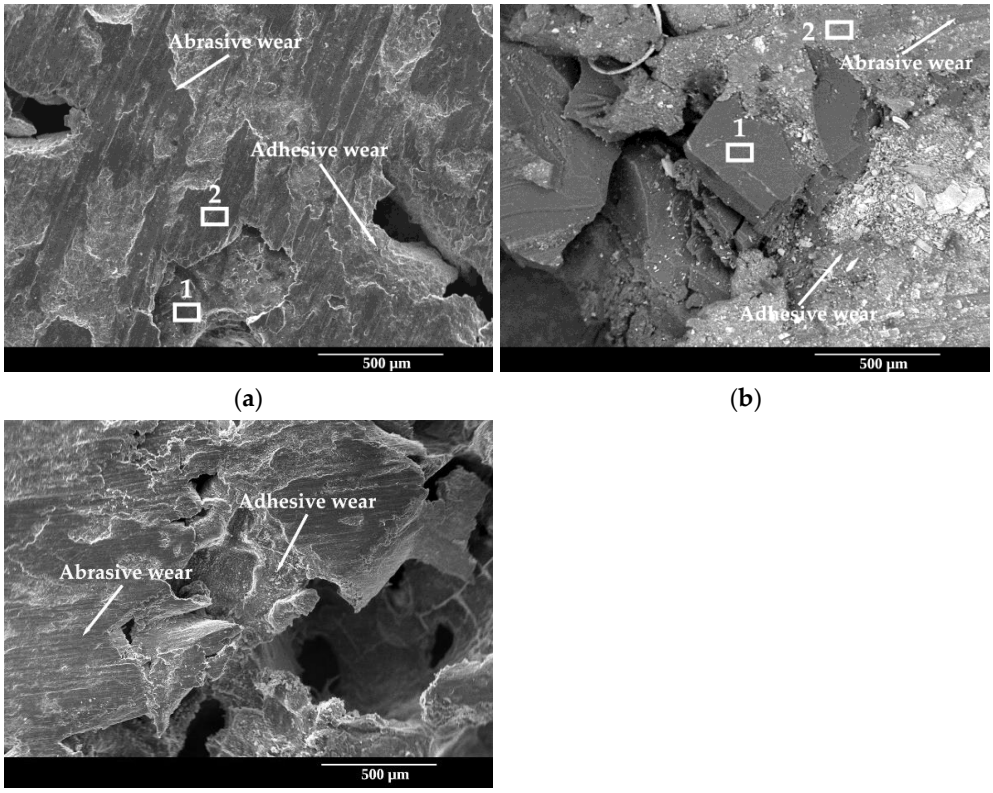


**Figure 3.** SEM images of post-tribological tests of two different materials: (**a**) AlSi10Mg material, low magnification, at ×87; (**b**) AlSi10Mg-SiC composite, high magnification, at ×300; (**c**) AlSi10Mg-SiC composite, low magnification, at ×81 with wear track and direction indicated.

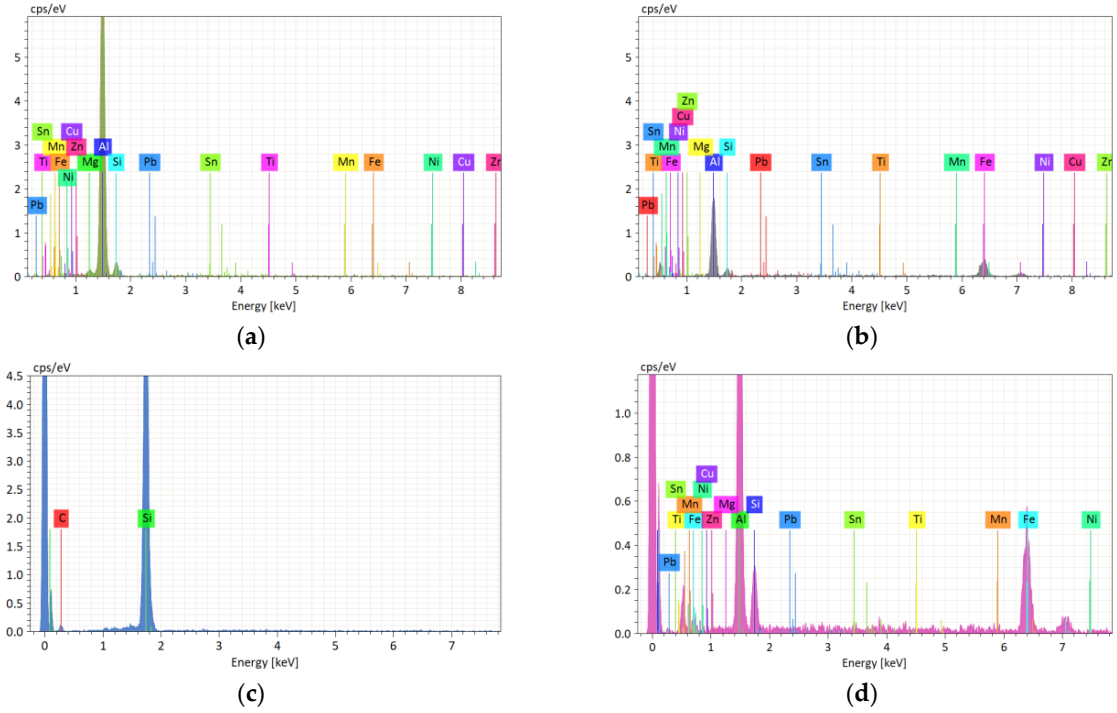


**Figure 4.** EDS spectra of post-tribological tests of two different materials: (**a**) related to Table 3, analysis 1, AlSi10Mg material; (**b**) related to Table 3, analysis 2, AlSi10Mg material; (**c**) related to Table 4, analysis 1, AlSi10Mg-SiC composite; (**d**) related to Table 4, analysis 2, AlSi10Mg-SiC composite.

After conducting a tribological experiment with a counter-steel body, the test specimen experienced abrasion and adhesion. The abrasion occurred when the sharp asperities on the surface of the steel body interacted with the surfaces of the AlSi10Mg material (skeleton) and AlSi10Mg-SiC (composite skeleton), causing the removal of material from the test pin surface in the form of wear debris. The primary wear mechanism observed under the specified load and linear speed was abrasive wear. This was suggested by the wear direction and wear scar observed on the contact zone indicated with an arrow in Figure 3a,b. The abrasive wear mechanism was expected to be more dominant due to the presence of pores in the material, which may have acted as stress concentrators and make the material more prone to abrasive wear.

Adhesion, on the other hand, occurs when the opposing surfaces come into direct contact and adhere to each other due to the attractive forces between them. During the tribological process, the tested pin surface experienced localized plastic deformation, which caused the surface to become rough and enhance the adhesion mechanism. As a result, material from the steel body was transferred to the AlSi10Mg material and the composite surface (refer to Figure 4a,b, and Tables 3 and 4), leading to adhesive and abrasive wear, shown with an arrow in Figure 3a,b.

The markings in Figure 3a highlight two zones in which the EDS analysis was conducted on a skeleton with pore sizes of 800 ÷ 1000 μm. The EDS-analysis results in Table 3 and the EDS spectra in Figure 4a indicate the presence of aluminum as the dominant peak in zone 1, followed by small peaks of Fe, Si, Mg, Cu, and Mn. The EDS-analysis results in Table 3 and the EDS spectra in Figure 4b indicate the presence of a secondary peak of iron in zone 2, which was caused by the interaction between the steel counterbody and the composite skeleton, resulting in the removal of material from both surfaces in the form of wear debris.

The findings from the first EDS analysis in Table 4 and the EDS spectra in Figure 4c suggest the incorporation of the SiC reinforcement into the pore walls of the composite skeleton. The second EDS analysis in Table 4 and the EDS spectra in Figure 4d indicate the presence of iron in the composite skeleton. This was due to the abrasion mechanism, which occurred when the sharp asperities on the surface of the steel counterbody interacted with the surface of the composite skeleton, causing the removal of material from the pin specimen's surface in the form of wear debris.

### *3.2. Wear Behavior*

The conducted pin-on-disk test of the porous open-cell-composite test specimen of AlSi10Mg reinforced with SiC particles, compared with the AlSi10Mg material under the test conditions of a load of 50 N and a linear speed of 1.0 $m \cdot s^{-1}$ at room temperature, showed that the composite skeleton had a lower coefficient of friction than the skeleton (as in Figure 5).

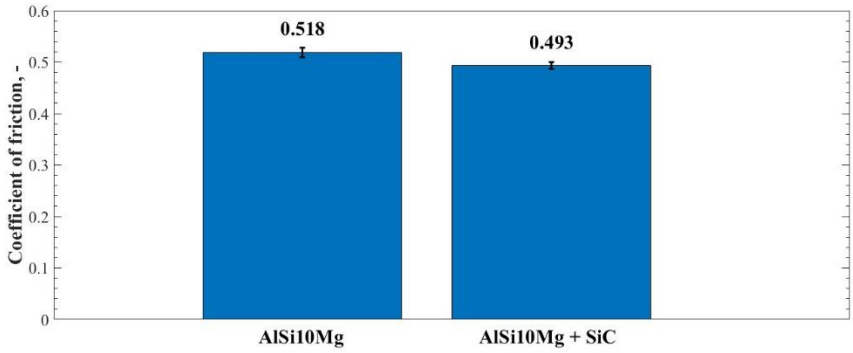


**Figure 5.** COF vs. sliding-distance test results for skeleton and composite skeleton at 50 N of load and 420 m of sliding distance under dry friction conditions at room temperature.

Specifically, the composite skeleton had a coefficient of friction of 0.493 (SEM = 0.0068), which was lower than the skeleton's coefficient of friction of 0.518 (SEM = 0.0096). Therefore, the composite skeleton showed a 4.82% improvement in terms of the coefficient of friction compared to the unmodified skeleton under the given testing conditions. This slight improvement suggests that the measured values for the coefficient of friction of the composite skeleton and the skeleton fell within the limits of the measurement error resulting from the scattering of the results.

The pin-on-disk test results showed that the composite skeleton had a mass wear of 2.3 mg (SEM = 0.36), while the skeleton had a mass wear of 6.7 mg (SEM = 0.29). Therefore, the mass wear of the composite skeleton was 65.7% lower than that of the skeleton under the given test conditions (refer to Figure 6). This indicates that the incorporation of the SiC reinforcement into the pore walls of the composite skeleton resulted in improved wear resistance compared to the unmodified skeleton. The SiC particles in the composite skeleton may have acted as reinforcements and improved the strength and wear resistance of the material. The lower mass wear in the composite skeleton may also have been due to the improved lubrication properties provided by the SiC particles, which may have reduced the contact and adhesion between the sliding surfaces, thereby reducing the wear. Overall, the results suggest that the porous open-cell composite test specimen of AlSi10Mg reinforced with SiC particles had superior tribological properties compared to the unmodified AlSi10Mg material.

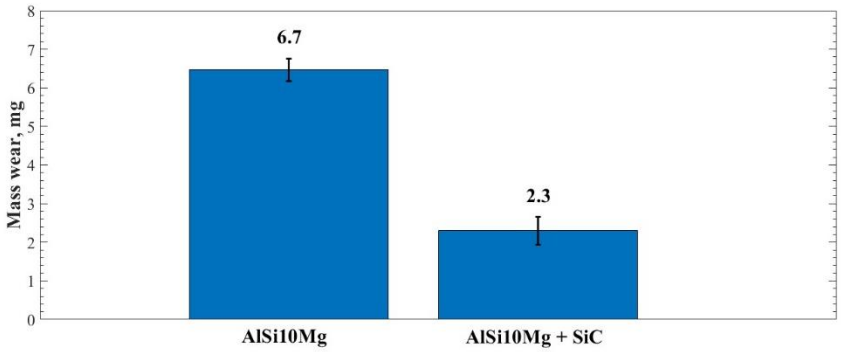


**Figure 6.** Mass wear of skeleton and composite skeleton at 50 N of load and 420 m of sliding distance under dry friction conditions at room temperature.

### *3.3. Prediction of the Coefficient of Friction*

Machine-learning algorithms were utilized to predict the COF of the AlSi10Mg-SiC composites under dry sliding conditions. The three different ML models, namely RF, DT, and XGB, were implemented to predict the wear behavior of the composites. The performances of these models were evaluated on the validation and test sets using various metrics, such as R2, RMSE, MSE, and MAE [50–52]. Table 5 provides the comparative performance results of the ML models in terms of their performance metrics on the test set, while Table 6 provides the comparative performance results of the ML models in terms of their performance metrics on the validation set.

**Table 5.** Test-set performance metrics.

| Metric Type | R2 | MSE | RMSE | MAE |
|---|---|---|---|---|
| **ML Model** | | **Score** | | |
| XGB | 0.9951 | 0.0000 | 0.0062 | 0.0045 |
| RF | 0.9393 | 0.0005 | 0.0219 | 0.0094 |
| DT | 0.7744 | 0.0018 | 0.0421 | 0.0198 |

**Table 6.** Validation-set performance metrics.

| Metric Type | R2 | MSE | RMSE | MAE |
|---|---|---|---|---|
| **ML Model** | | **Score** | | |
| XGB | 0.9907 | 0.0001 | 0.0122 | 0.0058 |
| RF | 0.9443 | 0.0008 | 0.0274 | 0.0116 |
| DT | 0.6562 | 0.0046 | 0.0681 | 0.0249 |

The coefficient of determination, or R2, is a statistical measure used to evaluate the performances of regression models in machine learning. It indicates how well the model fits the data by measuring the proportion of the variance in the dependent variable that can be described by the independent variables. The R2 value ranges from 0 to 1, where a value of 1 indicates that the model perfectly fits the data. The formula for R2 is as follows:

$$R2 = 1 - \frac{\sum_{i=1}^{n}(y_i - \hat{y}_i)^2}{\sum_{i=1}^{n}\left(y_i - \bar{y}\right)^2} \quad (1)$$

where:

n is the number of samples in the dataset;

$y_i$ is the actual value of the target variable for the i-th sample;

$\hat{y}_i$ is the predicted value of the target variable for the i-th sample;

$\bar{y}$ is the mean value of the target variable.

The MSE is a common metric employed to evaluate the performances of regression models. This metric calculates the mean of the squared differences between the predicted and actual values. The formula for the MSE is as follows:

$$MSE = \frac{1}{n}\sum_{i=1}^{n}(y_i - \hat{y}_i)^2 \quad (2)$$

where n, $y_i$, and $\hat{y}_i$ (i = 1, 2, . . . , n) are the same as in (1).

The RMSE is a metric used to evaluate the accuracy of a regression model. It calculates the square root of the average of the squared differences between the predicted and actual values, providing a measure of the average distance between the predicted and the actual values. The formula for the RMSE can be expressed as:

$$RMSE = \sqrt{\frac{1}{n}\sum_{i=1}^{n}\left(y_{i,pred} - y_{i,true}\right)^2} \quad (3)$$

where:

n is the number of samples;

$y_{i,pred}$ is the predicted value for the i-th sample;

$y_{i,true}$ is the actual value for the i-th sample.

The MAE is a metric used in regression analysis to determine the average absolute difference between the actual and predicted values. The calculation of the MAE can be expressed as:

$$MAE = \frac{1}{n}\sum_{i=1}^{n}|y_i - \hat{y}_i| \quad (4)$$

where n, $y_i$, and $\hat{y}_i$ (i = 1, 2, . . . , n) are the same as in (2).

To prevent the positive and negative errors from cancelling each other out, the absolute difference between the actual and predicted values was computed. The MAE score ranged from 0 to ∞, with lower values indicating better performance.

The results of our study demonstrate that the XGB algorithm outperformed the RF and DT algorithms in terms of both the test-set and the validation-set performance metrics. On the test set, the XGB achieved an R2 score of 99.51%, while the RF and the DT achieved R2

scores of 93.93% and 77.44%, respectively. The XGB also had the lowest MSE (0.0000) and RMSE (0.0062) values, indicating its superior predictive accuracy. On the validation set, the XGB and the RF showed similar performance levels, with R2 scores of 99.07% and 94.43%, respectively. The DT had a significantly lower R2 score, of 65.62%. However, the XGB still outperformed the RF in terms of MSE (0.0001 vs. 0.0008) and RMSE (0.0122 vs. 0.0274), while the RF had a slightly lower MAE value (0.0116 vs. 0.0058) compared to the XGB.

Overall, our results suggest that XGB is the best-performing algorithm for predicting the coefficient of friction based on the sliding distance measured, as it achieved the highest accuracy and lowest error values on both the test and the validation sets. These findings could have important implications for improving our understanding of tribological processes and may help to guide the development of more efficient lubrication strategies. The comparison of the performances of three machine-learning models in predicting the COF for the composite skeleton is presented in Figure 7.

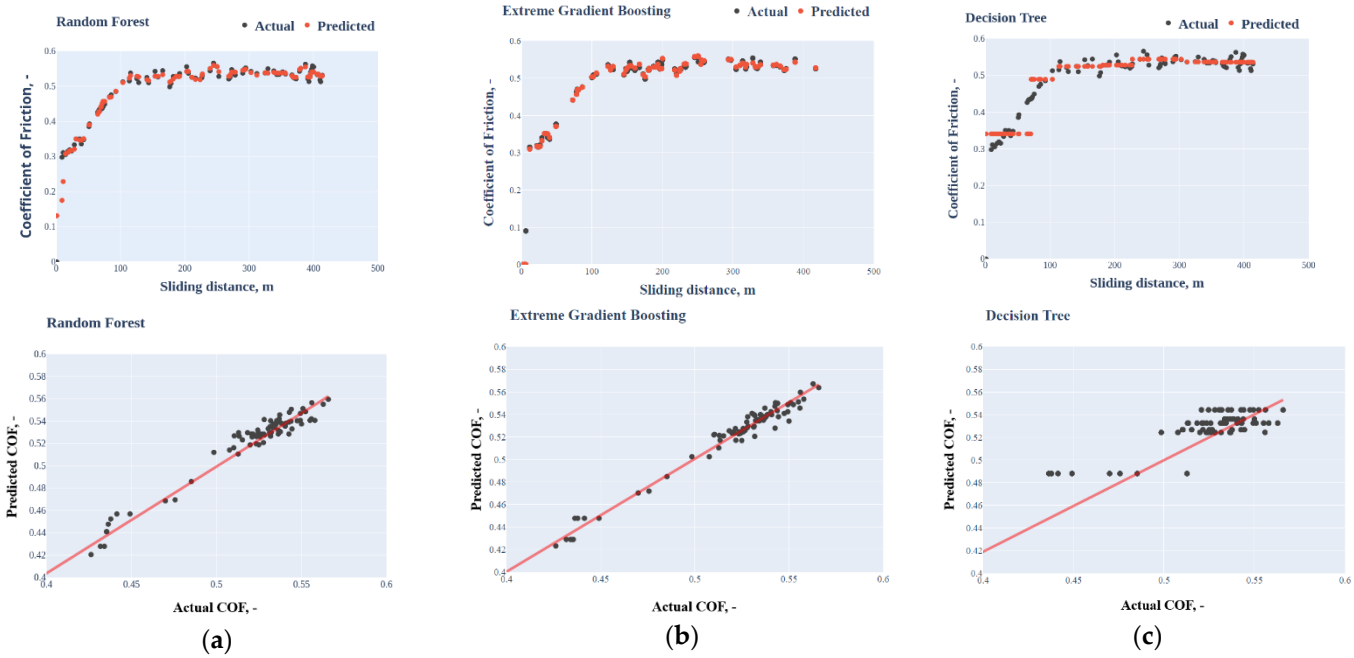


**Figure 7.** Comparison of the performances of three machine-learning models in predicting the coefficient of friction for a composite skeleton under dry sliding conditions at room temperature with a 50-N load, 1.0-m·s$^{-1}$ linear speed, and 420-m sliding distance. The figure displays the actual and predicted output values for each model. The models tested were: (**a**) Random Forest; (**b**) Extreme Gradient Boosting; and (**c**) Decision Tree.

## 4. Conclusions

This study investigated the tribological behavior of AlSi10Mg-SiC composites produced using a novel fabrication technique. The wear parameters, such as the mass wear and coefficient of friction, were evaluated using the pin-on-disk method under dry sliding-friction conditions at ambient temperature. The wear mechanisms were investigated using scanning-electron microscopy, while the elemental composition was examined using X-ray energy-dispersive spectroscopy. The incorporation of SiC reinforcement particles into the composite resulted in a 4.82% improvement in the coefficient of friction and a 65.7% reduction in the mass wear compared to the unmodified skeleton.

Machine-learning algorithms, namely Random Forest, Decision Tree, and Extreme Gradient Boosting, were utilized to predict the COF of the composites under dry sliding conditions. The performances of these ML models were evaluated on the validation and test sets using various metrics, such as R2, MSE, RMSE, and MAE. These results show that the Extreme Gradient Boosting model had the best performance on both the test set

and validation set, with the highest R2 and lowest RMSE and MAE values. The Random Forest model had the second-best performance, with moderately high R2 and RMSE values, but higher MSE and MAE than the Extreme Gradient Boosting model. The Decision Tree model had the worst performance on both sets, with the lowest R2 and highest MSE, RMSE, and MAE values. These results indicate that machine learning can be a valuable tool for predicting tribological behavior and optimizing composite materials.

In the future, we plan to expand our dataset and explore the correlations between technological and experimental variables based on the insights gained from this manuscript, with the goal of refining and improving our predictive model. In this way, we aim to enhance our understanding of the factors that affect the wear behavior of AMMCs and achieve more accurate and reliable predictions in the future.

The outcomes of this study have important implications for the development of high-performance composite materials. By incorporating SiC reinforcement particles, it is possible to enhance the tribological behavior of AlSi10Mg-SiC composites. The use of machine-learning algorithms can also provide valuable insights into the behavior of these materials and facilitate the development of optimized composite structures. Further research is needed to explore the potential of AlSi10Mg-SiC composites with different reinforcement-particle contents, as well as the application of machine-learning algorithms for predicting the tribological behavior of other composite materials. These efforts could lead to the development of new, high-performance materials with a wide range of industrial applications, including, but not limited to, the machinery and automotive industries.

**Author Contributions:** conceptualization, M.K. and L.D.; software, M.K. and V.P.; investigation, M.K. and V.P.; resources, L.D.; writing—original draft, M.K.; writing—review and editing, M.K.; supervision, L.D.; project administration, M.K.; funding acquisition, M.K. All authors have read and agreed to the published version of the manuscript.

**Funding:** This research was funded by the BULGARIAN NATIONAL SCIENCE FUND, Project КП-06-H57/20 "Fabrication of new type of self-lubricating antifriction metal matrix composite materials with improved mechanical and tribological properties".

**Acknowledgments:** We acknowledge the support of the European Regional Development Fund within the OP Science and Education for Smart Growth 2014–2020, Project CoE National Center of Mechatronics and Clean Technologies, BG05M2OP001-1.001-0008, in providing the necessary equipment for this work.

**Conflicts of Interest:** The authors declare no conflict of interest.

## References

1. Stanev, L.; Kolev, M.; Drenchev, B.; Drenchev, L. Open-Cell Metallic Porous Materials Obtained through Space Holders—Part II: Structure and Properties. A Review. *J. Manuf. Sci. Eng.* **2016**, *139*, 050802. [CrossRef]
2. Banhart, J. Manufacture, Characterisation and Application of Cellular Metals and Metal Foams. *Prog. Mater. Sci.* **2001**, *46*, 559–632. [CrossRef]
3. Parveez, B.; Jamal, N.A.; Maleque, A.; Yusof, F.; Jamadon, N.H.; Adzila, S. Review on Advances in Porous Al Composites and the Possible Way Forward. *J. Mater. Res. Technol.* **2021**, *14*, 2017–2038. [CrossRef]
4. Nathan, S.R.; Suganeswaran, K.; Kumar, S.; Thangavel, P.; Gobinath, V.K. Investigations on Microstructure, Thermo-Mechanical and Tribological Behavior of Graphene Oxide Reinforced AA7075 Surface Composites Developed via Friction Stir Processing. *J. Manuf. Process.* **2023**, *90*, 139–150. [CrossRef]
5. Samal, P.; Vundavilli, P.R.; Meher, A.; Mahapatra, M.M. Recent Progress in Aluminum Metal Matrix Composites: A Review on Processing, Mechanical and Wear Properties. *J. Manuf. Process.* **2020**, *59*, 131–152. [CrossRef]
6. Elizondo Luna, E.M.; Barari, F.; Woolley, R.; Goodall, R. Casting Protocols for the Production of Open Cell Aluminum Foams by the Replication Technique and the Effect on Porosity. *J. Vis. Exp.* **2014**, *94*, 52268. [CrossRef]
7. Bafti, H.; Habibolahzadeh, A. Compressive Properties of Aluminum Foam Produced by Powder-Carbamide Spacer Route. *Mater. Des.* **2013**, *52*, 404–411. [CrossRef]
8. Łazińska, M.; Durejko, T.; Lipiński, S.; Polkowski, W.; Czujko, T.; Varin, R.A. Porous Graded FeAl Intermetallic Foams Fabricated by Sintering Process Using NaCl Space Holders. *Mater. Sci. Eng. A* **2015**, *636*, 407–414. [CrossRef]
9. Golabgir, M.H.; Ebrahimi-Kahrizsangi, R.; Torabi, O.; Saatchi, A. Fabrication of Open Cell Fe-10%Al Foam by Space-Holder Technique. *Arch. Metall. Mater.* **2014**, *59*, 41–45. [CrossRef]

10. Golabgir, M.H.; Ebrahimi-Kahrizsangi, R.; Torabi, O.; Tajizadegan, H.; Jamshidi, A. Fabrication and Evaluation of Oxidation Resistance Performance of Open-Celled Fe(Al) Foam by Space-Holder Technique. *Adv. Powder Technol.* **2014**, *25*, 960–967. [CrossRef]
11. Hussain, Z.; Suffin, N.S.A. Microstructure and Mechanical Behaviour of Aluminium Foam Produced by Sintering Dissolution Process Using NaCl Space Holder. Available online: http://web.usm.my/jes/7_2011/JES-ART4-37-49.pdf (accessed on 8 March 2023).
12. Kolev, M.; Drenchev, L.; Stanev, L. Tribological Characterization of Aluminum/Babbitt Composites and Their Application to Sliding Bearing. *Arch. Foundry Eng.* **2020**, *20*, 31–36. [CrossRef]
13. Stanev, L.; Kolev, M.; Drenchev, L.; Krastev, B. Fabrication Technique and Characterization of Aluminum Alloy-Based Porous Composite Infiltrated with Babbitt Alloy. *J. Mater. Eng. Perform.* **2020**, *29*, 3767–3773. [CrossRef]
14. Esen, Z.; Bor, Ş. Characterization of Ti–6Al–4V Alloy Foams Synthesized by Space Holder Technique. *Mater. Sci. Eng. A* **2011**, *528*, 3200–3209. [CrossRef]
15. Mondal, D.P.; Patel, M.; Jain, H.; Jha, A.K.; Das, S.; Dasgupta, R. The Effect of the Particle Shape and Strain Rate on Microstructure and Compressive Deformation Response of Pure Ti-Foam Made Using Acrowax as Space Holder. *Mater. Sci. Eng. A* **2015**, *625*, 331–342. [CrossRef]
16. Xiang, C.; Zhang, Y.; Li, Z.; Zhang, H.; Huang, Y.; Tang, H. Preparation and Compressive Behavior of Porous Titanium Prepared by Space Holder Sintering Process. *Procedia Eng.* **2012**, *27*, 768–774. [CrossRef]
17. Michailidis, N.; Stergioudi, F.; Tsouknidas, A.; Pavlidou, E. Compressive Response of Al-Foams Produced via a Powder Sintering Process Based on a Leachable Space-Holder Material. *Mater. Sci. Eng. A* **2011**, *528*, 1662–1667. [CrossRef]
18. Parvanian, A.M.; Panjepour, M. Mechanical Behavior Improvement of Open-Pore Copper Foams Synthesized through Space Holder Technique. *Mater. Des.* **2013**, *49*, 834–841. [CrossRef]
19. Schmidt, A.; Siebeck, S.; Götze, U.; Wagner, G.; Nestler, D. Particle-Reinforced Aluminum Matrix Composites (AMCs)—Selected Results of an Integrated Technology, User, and Market Analysis and Forecast. *Metals* **2018**, *8*, 143. [CrossRef]
20. Surya, M.S.; Gugulothu, S.K. Fabrication, Mechanical and Wear Characterization of Silicon Carbide Reinforced Aluminium 7075 Metal Matrix Composite. *Silicon Chem.* **2022**, *14*, 2023–2032. [CrossRef]
21. Patel, M.; Sahu, S.K.; Singh, M.K. Abrasive Wear Behavior of SiC Particulate Reinforced AA5052 Metal Matrix Composite. *Mater. Today Proc.* **2020**, *33*, 5586–5591. [CrossRef]
22. Kumar Yadav, R.; Hasan, Z.; Husain Ansari, A. Investigation of Mechanical and Wear Behavior of Al Based SiC Reinforce Metal Matrix Composite. *Mater. Today Proc.* **2020**, *21*, 1537–1543. [CrossRef]
23. Aydin, F. The Investigation of the Effect of Particle Size on Wear Performance of AA7075/$Al_2O_3$ Composites Using Statistical Analysis and Different Machine Learning Methods. *Adv. Powder Technol.* **2021**, *32*, 445–463. [CrossRef]
24. Vijaya Bhaskar, K.; Sundarrajan, S.; Subba Rao, B.; Ravindra, K. Effect of Reinforcement and Wear Parameters on Dry Sliding Wear of Aluminum Composites—A Review. *Mater. Today Proc.* **2018**, *5*, 5891–5900. [CrossRef]
25. Stojanović, B. Application of Aluminium Hybrid Composites in Automotive Industry. *Teh. Vjesn.* **2015**, *22*, 247–251. [CrossRef]
26. Kumar Sharma, A.; Bhandari, R.; Aherwar, A.; Rimašauskienė, R.; Pinca-Bretotean, C. A Study of Advancement in Application Opportunities of Aluminum Metal Matrix Composites. *Mater. Today Proc.* **2020**, *26*, 2419–2424. [CrossRef]
27. Nayim, S.M.T.I.; Hasan, M.Z.; Seth, P.P.; Gupta, P.; Thakur, S.; Kumar, D.; Jamwal, A. Effect of CNT and TiC Hybrid Reinforcement on the Micro-Mechano-Tribo Behaviour of Aluminium Matrix Composites. *Mater. Today Proc.* **2020**, *21*, 1421–1424. [CrossRef]
28. Harti, J.I.; Prasad, T.B.; Nagaral, M.; Jadhav, P.; Auradi, V. Microstructure and Dry Sliding Wear Behaviour of Al2219-TiC Composites. *Mater. Today Proc.* **2017**, *4*, 11004–11009. [CrossRef]
29. Rajkumar, K.; Santosh, S. Effect of Nano and Micro Graphite Particle on Tribological Performance of Aluminium Metal Matrix Composites. *Appl. Mech. Mater.* **2014**, *592–594*, 917–921. [CrossRef]
30. Srinivasan, R.; Hariharan, K.; Jeyanthan, S.A.; Kamalesh, M.; Ali, I. Effect of Addition of Titanium Carbide and Graphite Reinforcement on Al7075 Hybrid Metal Matrix Composites by Gravity Stir Casting Method. *Mater. Today Proc.* **2022**, *62*, 86–93. [CrossRef]
31. Natrayan, L.; Senthil Kumar, M. Optimization of Wear Behaviour on AA6061/$Al_2O_3$/SiC Metal Matrix Composite Using Squeeze Casting Technique—Statistical Analysis. *Mater. Today Proc.* **2020**, *27*, 306–310. [CrossRef]
32. Sekar, K.; Ananda Rao, D.V. Investigation of Hybrid Composite A7075/SiC/$B_4C$ by Stir and Squeeze Casting Method. *Mater. Today Proc.* **2020**, *22*, 1398–1408. [CrossRef]
33. Vasanthakumar, P.; Sekar, K. Processing and Preparation of Aerospace-Grade Aluminium Hybrid Metal Matrix Composite in a Modified Stir Casting Furnace Integrated with Mechanical Supersonic Vibration Squeeze Infiltration Method. *Mater. Today Commun.* **2021**, *26*, 101732. [CrossRef]
34. Alizadeh, A.; Khayami, A.; Karamouz, M.; Hajizamani, M. Mechanical Properties and Wear Behavior of Al5083 Matrix Composites Reinforced with High Amounts of SiC Particles Fabricated by Combined Stir Casting and Squeeze Casting; A Comparative Study. *Ceram. Int.* **2022**, *48*, 179–189. [CrossRef]
35. Maleki, K.; Alizadeh, A.; Hajizamani, M. Compressive Strength and Wear Properties of SiC/Al6061 Composites Reinforced with High Contents of SiC Fabricated by Pressure-Assisted Infiltration. *Ceram. Int.* **2021**, *47*, 2406–2413. [CrossRef]
36. Jiang, W.; Zhu, J.; Li, G.; Guan, F.; Yu, Y.; Fan, Z. Enhanced Mechanical Properties of 6082 Aluminum Alloy via SiC Addition Combined with Squeeze Casting. *J. Mater. Sci. Technol.* **2021**, *88*, 119–131. [CrossRef]

37. Yuan, D.; Yang, X.; Wu, S.; Lü, S.; Hu, K. Development of High Strength and Toughness Nano-SiCp/A356 Composites with Ultrasonic Vibration and Squeeze Casting. *J. Mater. Process. Technol.* **2019**, *269*, 1–9. [CrossRef]
38. Chakkravarthy, V.; Lakshmanan, M.; Manojkumar, P.; Prabhakaran, R. Crystallographic Orientation and Wear Characteristics of TiN, SiC, Nb Embedded Al7075 Composite. *Mater. Lett.* **2022**, *306*, 130936. [CrossRef]
39. Kota, N.; Jana, P.; Sahasrabudhe, S.; Roy, S. Processing and Characterization of Al-Si Alloy/SiC Foam Interpenetrating Phase Composite. *Mater. Today Proc.* **2021**, *44*, 2930–2933. [CrossRef]
40. Swetlana, S.; Khatavkar, N.; Singh, A.K. Development of Vickers Hardness Prediction Models via Microstructural Analysis and Machine Learning. *J. Mater. Sci.* **2020**, *55*, 15845–15856. [CrossRef]
41. Liu, J.; Zhang, Y.; Zhang, Y.; Kitipornchai, S.; Yang, J. Machine Learning Assisted Prediction of Mechanical Properties of Graphene/Aluminium Nanocomposite Based on Molecular Dynamics Simulation. *Mater. Des.* **2022**, *213*, 110334. [CrossRef]
42. He, P.; Liu, Q.; Kruzic, J.J.; Li, X. Machine-Learning Assisted Additive Manufacturing of a TiCN Reinforced AlSi10Mg Composite with Tailorable Mechanical Properties. *Mater. Lett.* **2022**, *307*, 131018. [CrossRef]
43. Kolev, M.; Drenchev, L.; Petkov, V.; Dimitrova, R. Production and Tribological Characterization of Advanced Open-Cell AlSi10Mg-$Al_2O_3$ Composites. *Metals* **2023**, *13*, 131. [CrossRef]
44. Kolev, M.; Drenchev, L.; Petkov, V. Wear Analysis of an Advanced Al–$Al_2O_3$ Composite Infiltrated with a Tin-Based Alloy. *Metals* **2021**, *11*, 1692. [CrossRef]
45. Stanev, L.; Kolev, M.; Drenchev, L. Enhanced Tribological Properties of an Advanced Al–$Al_2O_3$ Composite Infiltrated with a Tin-Based Alloy. *J. Tribol.* **2021**, *143*, 064502. [CrossRef]
46. Aydin, F.; Durgut, R.; Mustu, M.; Demir, B. Prediction of Wear Performance of ZK60/$CeO_2$ Composites Using Machine Learning Models. *Tribol. Int.* **2023**, *177*, 107945. [CrossRef]
47. Charbuty, B.; Abdulazeez, A. Classification Based on Decision Tree Algorithm for Machine Learning. *J. Appl. Sci. Technol. Trends* **2021**, *2*, 20–28. [CrossRef]
48. Breiman, L. Random Forests. *Mach. Learn.* **2001**, *45*, 5–32. [CrossRef]
49. Chen, T.; Guestrin, C. *XGBoost: A Scalable Tree Boosting System*; Association for Computing Machinery: New York, NY, USA, 2016.
50. He, Z.; Shi, T.; Xuan, J.; Li, T. Research on Tool Wear Prediction Based on Temperature Signals and Deep Learning. *Wear* **2021**, *478–479*, 203902. [CrossRef]
51. Aydin, F.; Durgut, R. Estimation of Wear Performance of AZ91 Alloy under Dry Sliding Conditions Using Machine Learning Methods. *Trans. Nonferrous Met. Soc. China* **2021**, *31*, 125–137. [CrossRef]
52. Chicco, D.; Warrens, M.J.; Jurman, G. The Coefficient of Determination R-Squared Is More Informative than SMAPE, MAE, MAPE, MSE and RMSE in Regression Analysis Evaluation. *PeerJ Comput. Sci.* **2021**, *7*, e623. [CrossRef]